ARTICLE

Few-Layer Graphene as a Support Film for Transmission Electron Microscopy Imaging of Nanoparticles

James R. McBride,[†] Andrew R. Lupini,[‡] Michael A. Schreuder,[†] Nathanael J. Smith,[§] Stephen J. Pennycook,[‡] and Sandra J. Rosenthal*[,†,||]

Department of Chemistry, Department of Physics and Astronomy, Department of Pharmacology, and Department of Chemical and Biomolecular Engineering, Vanderbilt University, Nashville, Tennessee 37235, Oak Ridge National Laboratory, Materials Science and Technology Division, Oak Ridge, Tennessee 37831, and Department of Physics and Astronomy, Middle Tennessee State University, Murfreesboro, Tennessee 37132

ABSTRACT One consistent limitation for high-resolution imaging of small nanoparticles is the high background signal from the amorphous carbon support film. With interest growing for smaller and smaller nanostructures, state of the art electron microscopes are becoming necessary for rudimentary tasks, such as nanoparticle sizing. As a monolayer of carbon, free-standing graphene represents the ultimate support film for nanoparticle imaging. In this work, conventional high-resolution transmission electron microscopy (HRTEM) and aberration-corrected scanning transmission electron microscopy (STEM) were used to assess the benefits and feasibility of few-layer graphene support films. Suspensions of few-layer graphene to produce the support films were prepared by simple sonication of exfoliated graphite. The greatest benefit was observed for conventional HRTEM, where lattice resolved imaging of sub 2 nm CdSe nanocrystals was achieved. The few-layer graphene films were also used as a support film for C_s-corrected STEM and electron energy loss spectroscopy of $CuInSe_2$ nanocrystals.

KEYWORDS: graphene • few-layer graphene • transmission electron microscopy • aberration-corrected scanning transmission electron microscopy • nanocrystal • nanoparticle • cadmium selenide • copper indium selenide,

INTRODUCTION

Transmission electron microscopy (TEM) and scanning transmission electron microscopy (STEM) are heavily relied upon for nanomaterials characterization. Both are used extensively for nanoparticle characterization, due to their reliability in measuring nanoparticle size and shape, as well as offering elemental analysis through energy dispersive spectroscopy (EDS) and electron energy loss spectroscopy (EELS) (1−7). However, conventional TEM only excels at imaging nanocrystals with diameters larger than 3 nm that are free from excess surfactants. It can become very challenging to obtain an image when the nanocrystal becomes much smaller and is composed of a low-Z material (8−14). In this size regime, contrast from the amorphous carbon support film is often on the order of or greater than that of the nanocrystal. As a result, one of the major limitations of imaging low-contrast materials is the high background from the amorphous carbon support. Although dark field imaging techniques can remove most of the carbon background, this is done at the expense of signal strength. To combat this effect, amorphous carbon films as thin as 3 nm are commercially available. Here, we report the first application of few-layer graphene as support films for nanocrystal imaging. The films provided nearly background-free imaging for conventional HRTEM and are suitable for atomic resolution STEM imaging and EELS.

The recent discovery and development of free-standing graphene sheets has raised the possibility of their use as alternative support films to amorphous carbon substrates. Graphene is the atomically thin form of graphite. Few-layer graphene is used to describe stacks of more than one sheet and is synonymous with ultrathin graphite (15). Graphene is an ideal support film for electron microscopy, since it is atomically thin, relatively flat, and highly conductive. The potential for graphene as a support film was made clear in an extraordinary fashion by Meyer et al., who detected single oxygen and hydrogen adatoms using a conventional HRTEM (16, 17). This advance could lead to the facile imaging of small inorganic clusters or amorphous organic structures without staining, and quite possibly imaging the surfactant coverage. However, with the exception of Booth et al., who imaged copper nanoparticles, and Lee et al., who have recently imaged the surface ligands of gold nanoparticles, the majority of electron microscopy efforts have been centered on studying the structure of graphene and graphene oxide (18−23).

Obtaining single- and few-layer graphene is typically achieved by rubbing carbon onto a silicon wafer and using an optical microscope to identify the locations of very thin

* To whom correspondence should be addressed. E-mail: Sandra.j.rosenthal@vanderbilt.edu.
Received for review September 8, 2009 and accepted October 23, 2009
[†] Department of Chemistry, Vanderbilt University.
[‡] Oak Ridge National Laboratory.
[§] Middle Tennessee State University.
[||] Department of Physics and Astronomy, Department of Pharmacology, and Department of Chemical and Biomolecular Engineering, Vanderbilt University.
DOI: 10.1021/am900608j

Published on Web 11/03/2009

pieces (24−26). Although useful for identifying large sheets of only few-layer or single-layer graphene, this process is not conducive to producing a large number of support films quickly. Alternatively, there are a variety of other techniques to produce few-layer graphene, including ball milling of graphite, solvothermal, large-scale via a gas-phase synthesis, plasma- and microwave-enhanced chemical vapor deposition, and the reduction of graphene oxide suspensions (27−34). However, as a support film for nanoparticles, large areas of single-layer graphene are not necessary and the technique should be simple enough to allow for the production of a large number of films at a time.

A method was developed by Hernandez et al. that simply used organic solvents to exfoliate graphite (35). Blake et al. followed this work by utilizing a common organic solvent, dimethylformamide, to produce films of graphene flakes with the aid of sonication (36). After 3 h of sonication, the solution turns a dark gray with pieces of graphene and few-layer graphene in solution. This solution can then be centrifuged to remove any large pieces, leaving only very small flakes in solution. Afterward, it can be drop-cast onto any substrate to deposit large areas of thin films of few-layer graphene. Here, we use a modified version of this method to produce few-layer and single-layer graphene support films. Standard and ultrasmall CdSe nanocrystals were imaged using conventional HRTEM and C_s-corrected STEM. The reduced background from the few-layer graphene films allows for clear lattice-resolved images of sub 2 nm CdSe to be obtained under conventional HRTEM conditions. The films were also used to obtain EELS images of $CuInSe_2$ nanocrystals, with enough detail to see both the nanocrystal core and the organic capping ligands. Our results indicate that widespread use of graphene support films will greatly enhance conventional HRTEM and STEM/EELS imaging of nanoparticles.

EXPERIMENTAL SECTION

Synthesis and Rutherford Backscattering Spectroscopy of Nanocrystals. CdSe nanocrystals were prepared by following the synthesis of Bowers et al. and purified by precipitation with two cycles of the previously described methanol/hexanol/methanol precipitation procedure (37). $CuInSe_2$ nanocrystals were synthesized following the method of Panthani et al. and were purified by three consecutive toluene/acetone precipitations (38). Rutherford backscattering spectroscopy was performed to determine the stoichiometry of the Cu−In−Se nanocrystals, which was measured to be $Cu_{11}In_6Se_8$. Samples were prepared by dropping dilute solutions of the purified nanocrystals onto pyrolitic graphite and were analyzed using a 1.8 MeV He ion beam. The high copper content determined by RBS is likely the result of unreacted precursors remaining in solution after purification. Allen et al. have discussed the possibility of a variety of possible stoichiometries for Cu−In−Se; however, none were copper rich (39).

General Comment on Nanoparticle Purification from Organic Surfactants for HRTEM/STEM. One of the primary difficulties in nanoparticle sample preparation is the removal of excess surfactants and oily solvents. This excess material not only greatly reduces contrast in HRTEM imaging but can be a source of severe contamination. Contamination buildup can be exacerbated by the high current per unit area found under STEM imaging conditions, making sample purity crucial. Organic material deposited with the nanoparticles can be easily seen on few-layer graphene by a noticeable increase in film thickness and a loss of the crystalline appearance of the film.

In the past, tri-*n*-octylphosphine oxide (TOPO) coated nanoparticles were simple to purify by consecutive precipitations with methanol. However, modern synthetic techniques utilize a mixture of long-chain alkylamine powders, such as hexadecylamine (HDA), and oils such as octadecene, oleic acid, and oleylamine. As a result, nanoparticle purification has become more complicated. To remove organometallic salts and suspended surfactants, a reverse precipitation step is needed where the nanoparticles are dispersed in a solvent in which they are slightly soluble (e.g., long-chain alcohols), followed by 30 min of centrifugation at 6k rpm. The nanoparticle supernatant is then separated from the precipitated surfactants and mixed with a polar solvent for collection via further centrifugation. The removal of oils requires a delicate balance of nonpolar solvents (e.g. toluene and hexanes) to mix with the oils and polar solvents (e.g. methanol and acetone) to precipitate the nanoparticles. The oils are somewhat miscible in the nonpolar/polar mixture, facilitating separation of the oils from the nanoparticles. After several washing iterations, the solubility of the nanoparticles can become compromised due to the loss of surface ligands. As new synthetic techniques are attempted, it may be necessary to split the sample into two aliquots prior to purification. This allows for the determination of the maximum number of washing cycles that can be performed with half of the material, while leaving the other half for cleaning and use.

Preparation of Few-Layer Graphene Support Films. Graphite flakes were obtained by gently pressing masking tape onto a freshly cleaved highly ordered pyrolytic graphite (HOPG) surface (SPI# 436HP-AB). The tape was then slowly removed, leaving behind raised flakes of graphite on the HOPG surface. To limit glue contamination, graphite flakes that were attached to the tape were not used. Tweezers were then used to peel off continuous sheets of graphite, with an area of approximately 3 mm^2. Two sheets were placed into a small vial with 2 mL of toluene. The graphite−toluene solution was then sonicated (Branson 3210) for 3 h or until the majority of the graphite was dissolved. The solutions could be centrifuged to remove larger pieces of graphite, although this was not necessary for our purposes. Nanocrystal samples were prepared by first depositing a suspension of sonicated graphite flakes in toluene onto a lacey carbon support film (Ted Pella Inc., Item No. 1883-F) and allowing it to dry, followed by the addition of a drop of dilute nanocrystals in toluene or hexanes.

Electron Microscopy. Conventional HRTEM images were obtained using a Phillips CM20 200 kV TEM with a LaB_6 emission source and fitted with a 2K × 2K CCD camera from AMT. Z-STEM images and EELS spectra of the $CuInSe_2$ nanocrystals were collected using the VG603U 300 kV STEM fitted with a C_s-corrector from Nion and an Enfina EELS spectrometer, while Z-STEM images of the CdSe nanocrystals were obtained using a 300 kV C_s-corrected Titan. Images were smoothed to reduce noise using DigitalMicrograph. EELS spectra were collected in the range from 0 to 1450 eV with an energy resolution of ∼1 eV. In order to improve signal to noise, the beam current was increased at the expense of spatial resolution. The background-subtracted edge intensities were plotted with 50 eV windows for indium and carbon, while a 200 eV window was used for copper.

RESULTS AND DISCUSSION

Initially, we applied the DMF method to depositing dilute solutions of few-layer graphene onto lacey carbon support films (36). Coverage can be controlled by adjusting the solution concentration and the size of the drop. Once in the TEM, the characteristic diffraction pattern for graphite mixed

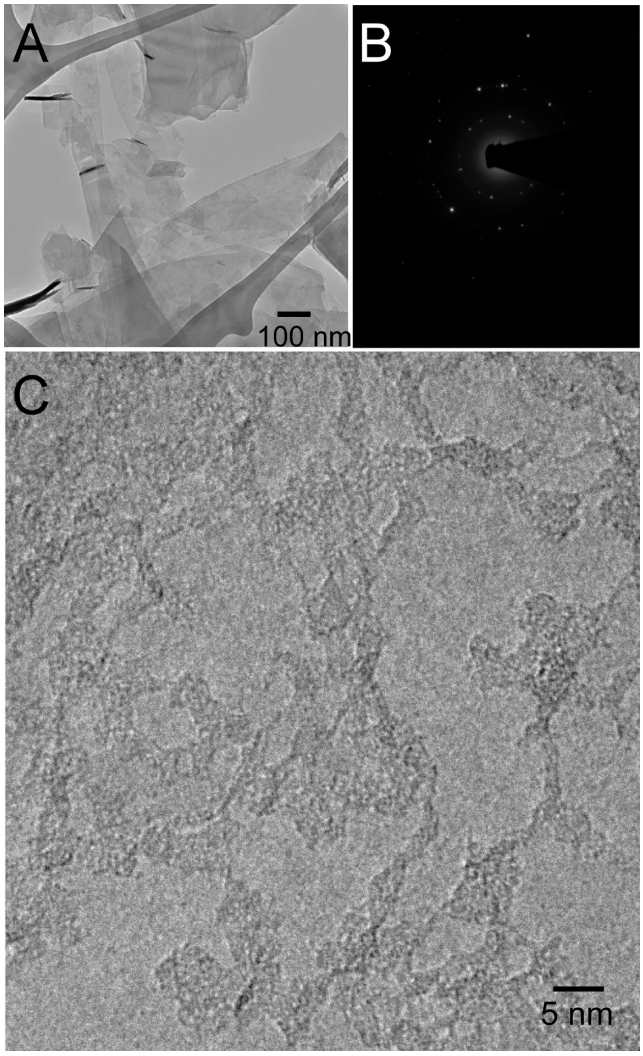

FIGURE 1. Few-layer graphene films: (A) flakes of few-layer graphene on a holey carbon TEM grid; (B) selective area diffraction pattern of the few-layer graphene film, showing its crystallinity; (C) high-magnification view of a piece of graphene with carbonaceous debris coating the surface.

with few-layer graphene was observed. However, the diffraction pattern would quickly fade, indicating the film was becoming amorphous while being illuminated.

This was likely due to residual DMF reacting with the graphene under the electron beam. When toluene was used in place of DMF, the films remained stable under continuous illumination. Similar results were seen with hexanes and benzene, and a paper recently published by Warner et al. uses a similar process with dichloromethane (40).

Figure 1A shows a low-magnification TEM image of the as-prepared films. The graphite deposits appear as layered sheets with few-layer and single-layer graphene dispersed throughout. The graphene sheets generally consist of varying amounts of clean surfaces surrounded by carbonaceous debris. Figure 1B is a selected area electron diffraction pattern showing the characteristic diffraction for few-layer graphene. Figure 1C is a high-magnification TEM image of a piece of graphene coated with carbonaceous debris. The amount of debris and the appearance of pure graphene regions are similar to those seen by Meyer et al. (16).

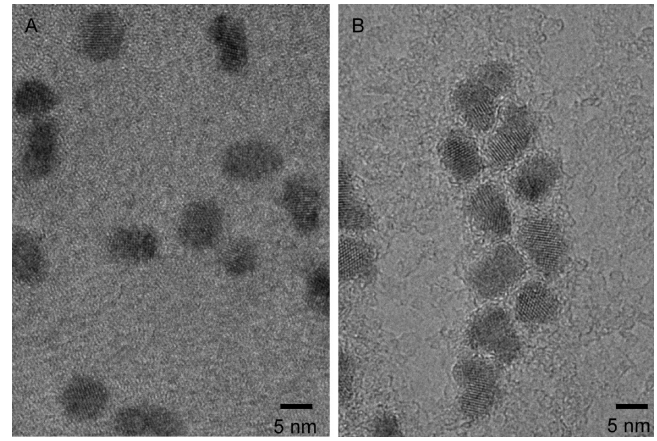

FIGURE 2. Comparison of support films using HRTEM: (A) 5 nm CdSe deposited on an ultrathin coated carbon grid; (B) 5 nm CdSe deposited onto a few-layer graphene support film, showing the nanocrystals adhering to the surface debris. Despite the debris, the surfaces of the nanocrystals are much sharper on the few-layer graphene film.

Parts A and B of Figure 2 are a comparison of HRTEM images of a single sample of CdSe nanocrystals acquired at the same magnification on different support films. Figure 2A was prepared using an ultrathin carbon support film, which is commercially available from Ted Pella (Item No. 1822-F).

Figure 2B was prepared using a few-layer graphene support film. The most striking difference between the two images is the near-featureless background of the graphene support. This allows for the surface to be unambiguously measured, as it is clear and distinct from the support film. Also, the lattice images have fewer artifacts from the support film. However, there are features that resemble "spaghetti" that are associated with the nanocrystals. Although these features seem to be attached to the nanocrystals, it very well may be the reverse; the nanocrystals may be adhering more strongly to imperfect surface patches and clustering together as the solvent evaporates. Graphene edges and surface imperfections would have more sites which the nanocrystals could adhere to, in the same way that adatoms tend to be found at step edges.

Another possibility is that this "spaghetti" is an unreacted precursor that often remains after nanocrystal purification. Free metal oxides and organometallic precursors are difficult to completely eliminate using precipitation techniques, as has been observed using Rutherford backscattering spectroscopy (41). This material, including single atoms, has been seen in aberration-corrected STEM images (13). However, without the low background afforded by the graphene support, this material would be invisible using conventional TEM. Thus, the low background level of few-layer graphene could have important implications, since the detection and elimination of these contaminants are critical for the development of nanocrystal-based devices.

There is a growing interest in developing ultrasmall nanocrystals as a subclass of nanocrystals. One reason for this is that fluorescent quantum dots utilizing ultrasmall cores have been demonstrated to behave differently in vitro compared to conventional 8−10 nm

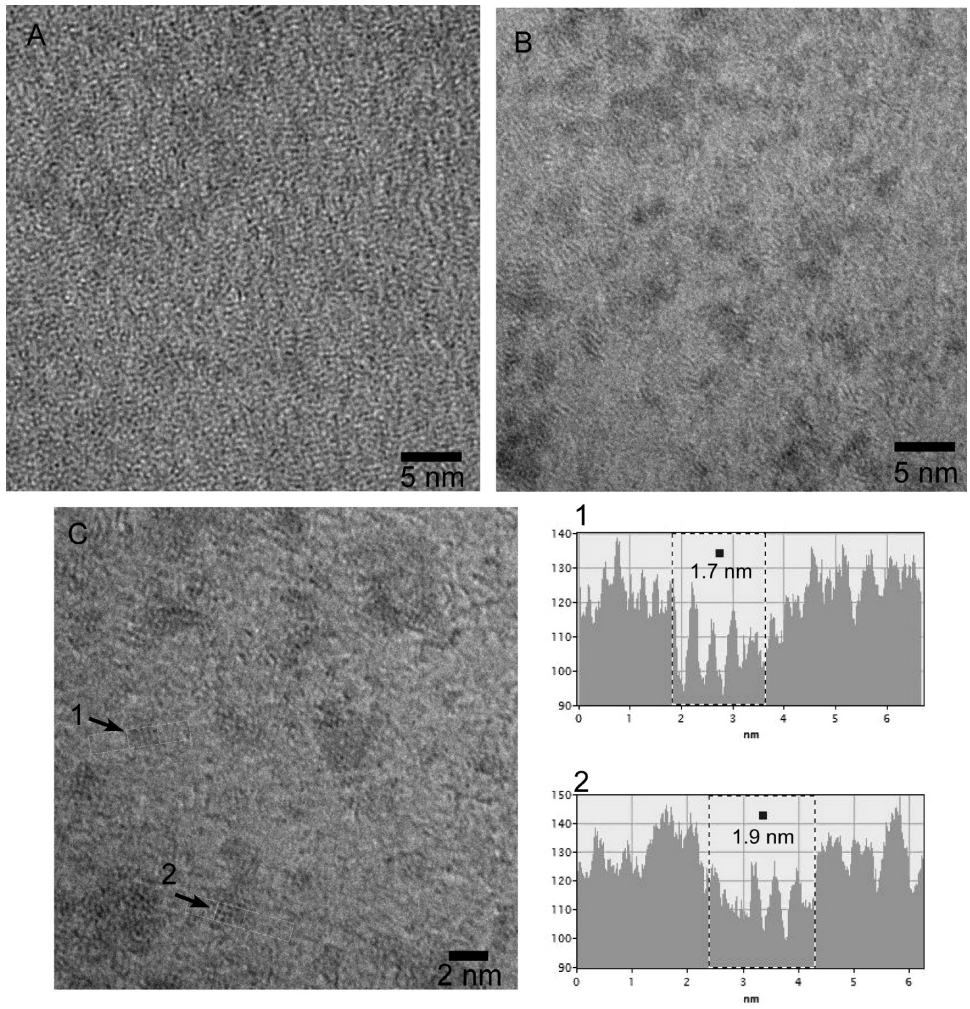

FIGURE 3. HRTEM imaging of ultrasmall CdSe on few-layer graphene: (A) practically invisible ultrasmall CdSe nanocrystals on an ultrathin carbon coated support grid; (B) the same ultrasmall nanocrystals becoming identifiable on the graphene support film; (C) higher magnification image showing several sub 2 nm nanocrystals with lattice fringes. The intensity profiles (right) were used to determine the diameter for the nanocrystals marked "1" and "2".

quantum dots (42). Another is that the photoluminescence of ultrasmall CdSe exhibits a strikingly white emission that has potential uses in solid-state-lighting applications (37). From a more fundamental aspect, under certain conditions very small nanocrystals can behave like magic clusters, with ultrastable sizes that are resistant to growth (8, 10, 12, 43, 44). It is believed that these magic size nanocrystals exhibit a unique "closed shell" structure (44). A need has therefore arisen to characterize the structure of ultrasmall nanocrystals. However, imaging ultrasmall nanocrystals using HRTEM is extremely challenging, due to the extreme lack of contrast. Since there are only two to five lattice planes, fringes are extremely difficult to distinguish from the random fluctuations of the amorphous carbon background. Any structural disorder may eliminate any lattice fringes entirely. Additionally, the nanocrystal diameter is on the order of the carbon chain length of the surface ligands, further reducing the amount of contrast in HRTEM. With the exception of the aberration-corrected Z-STEM image of a pair of ultrasmall nanocrystals (37), the structure of ultrasmall and magic size nanocrystals has been limited to theoretical treatments (44–48).

Figure 3 shows HRTEM images of sub 2 nm nanocrystals on a traditional ultrathin carbon support (Figure 3A) and few-layer graphene (Figure 3B). While very little can be discerned from the image in Figure 3A, there is enough contrast and clarity in Figure 3B to identify the presence of ultrasmall nanocrystals. The size (1.7 and 1.9 nm) and shape of two of the nanocrystals (indicated by arrows in Figure 3C) are clearly discernible. The lattice spacing is consistent with either zinc blende or wurtzite CdSe. Additionally, contrast between precursors and aggregated nanocrystals can be seen, similar to that obtained using an aberration-corrected 300 kV Titan with sub-angstrom resolution (13).

Graphene support films also have great potential in modern, aberration-corrected STEM imaging. In Z-contrast or high angle annular dark field (HAADF) imaging, only the highly scattered electrons are used to form an image, essentially removing the carbon background from the image as well as providing a directly interpretable image. There-

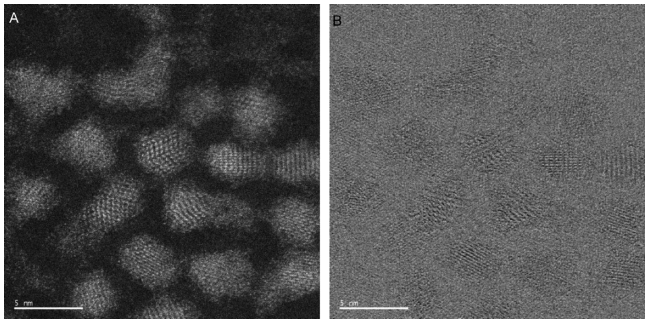

FIGURE 4. C_s-corrected Z-STEM imaging of CdSe nanocrystals: (A) Z-STEM image of 5 nm CdSe nanocrystals on few-layer graphene; (B) simultaneous BF image showing near-featureless background, with the exception of faint graphite fringes.

fore, other than a slight broadening of the electron beam, the thickness of the carbon support film in Z-STEM imaging is less important. However, graphene does provide potential benefits for bright field (BF) STEM similar to that of HRTEM.

Figure 4 contains aberration-corrected STEM images of CdSe nanocrystals on few-layer graphene. The Z-STEM image in Figure 4A shows little improvement over images previously obtained using conventional films (7). The background shows the presence of single atoms and a faint coating of organics. However, the bright field STEM image (Figure 4B) has a very low background, with only faint fringes from the graphene.

It was unclear how stable the graphene would be with the combination of nanoparticles and the highly focused electron beam used in STEM imaging. Under these imaging conditions, the nanocrystals typically began to disintegrate while the graphene support remained quite stable. After a few scans over the same area, the graphene would slowly become amorphous, as observed by the loss of carbon fringes in the BF image. The beam will also produce a hole in the film if left in a single position for more than a few seconds, which is similar to the behavior of with traditional carbon supports.

Electron energy loss spectra (EELS) reveal the energy lost by inelastically scattered electrons as they are transmitted through the sample. Since EELS scattering angles are small, these spectra can be obtained simultaneously with the Z-STEM image and may greatly benefit from an atomically thin support film. Currently, EELS spectroscopy on nanoparticles is difficult, due to the high background signal from the carbon support (3, 49, 50). The ideal solution is to measure the EELS spectrum of the particle over a hole. However, this is impractical for particles with length dimensions less than 10 nm. Being only 1 atom thick, a graphene support should have far less background, improving the overall signal-to-noise ratio.

Z-STEM and EELS were used to characterize $CuInSe_2$ nanocrystals on few-layer graphene. $CuInSe_2$ nanocrystals have potential uses as near-IR emitters as well as light harvesters for photovoltaic applications (39, 51, 52). As with other alloy systems, there is a possibility for the formation of core/shell structures or a subspecies of nanocrystals containing only part of the constituent atoms (5, 53). Figure 5A is an atomic resolution Z-STEM image of $CuInSe_2$ on a graphene support film. The relatively uniform intensity over the entire nanocrystal suggests that the alloy is homogeneous. Figure 5B gives a simultaneously acquired BF image, showing the same nanocrystal with the structure of the graphene support in the background. The carbonaceous debris is evident in both images. Figure 5C is a representative EELS spectrum acquired over a single $CuInSe_2$ nanocrystal, showing the indium and copper edges as well as a weak selenium edge. Figure 5D shows the region where the EELS spectral images were collected. The image resolution is noticeably less than for the Z-STEM image, due to the high current setting and long dwell times used to improve the EELS signal. The EELS spectrum images for carbon, indium, and copper are shown in Figure 5E. The EELS image for the carbon edge is clearly picking up an increase in carbon signal around the nanocrystals, which is likely from ligands bound to the nanocrystal surface. Two of the smaller nanocrystals fail to show up in the copper image, suggesting that they are exclusively indium. This observation is surprising, given that Rutherford backscattering spectroscopy suggests the sample

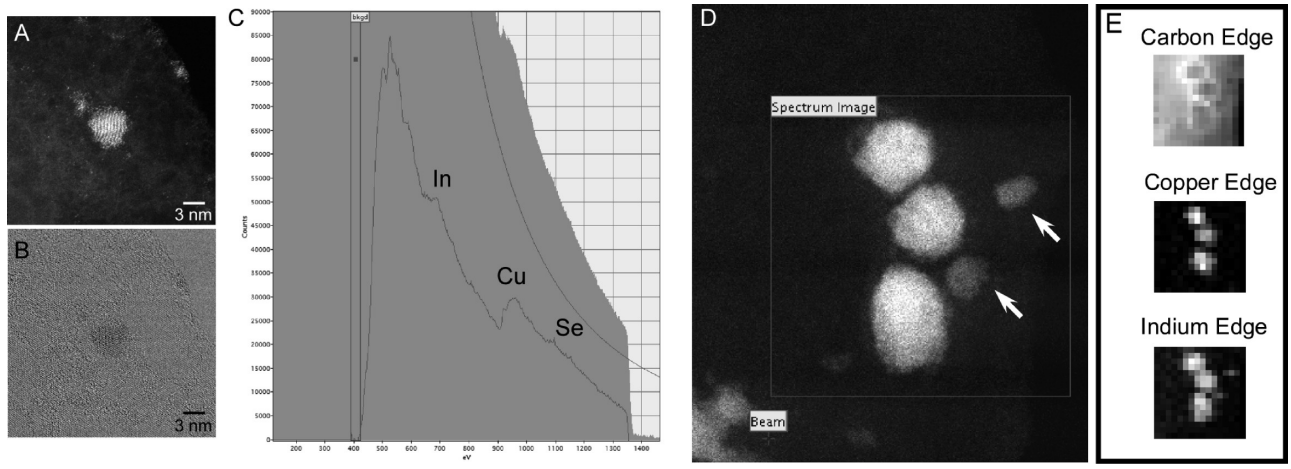

FIGURE 5. EELS analysis of $CuInSe_2$ on few-layer graphene: (A, B) Z-STEM and BF images of a $CuInSe_2$ nanocrystal on few-layer graphene; (C) representative EELS spectrum collected over a single $CuInSe_2$ nanocrystal; (D) region where an EELS spectrum image was collected with the elemental images shown in (E). The two nanocrystals marked by arrows in (D) appear only in the indium edge spectrum image.

is copper rich. We note that quantitative analysis of these EELS signals is particularly difficult, due to the low intensity and shape of their respective edges. Additionally, some of the improvement of the carbon support may be negated by the thick ligand coverage on the nanocrystals. However, the film was extremely resilient to the high current setting and long dwell times required for detailed EELS analysis, most likely due to the high conductive of graphene.

CONCLUSION

The images obtained using conventional HRTEM and modern aberration-corrected Z-STEM have shown a glimpse into the potential for graphene as a support film. In addition to an overall improved image contrast for traditional nanocrystals, few-layer graphene films facilitated the imaging of sub 2 nm CdSe nanocrystals using conventional HRTEM by nearly eliminating the background signal from the support film. Z-STEM/EELS images of the structure and chemical composition of $CuInSe_2$ nanocrystals were also obtained using few-layer graphene as a support film. While little improvement was possible for Z-STEM imaging using few-layer graphene supports in comparison to traditional carbon supports, EELS imaging using the few-layer graphene as a support did benefit from the lower carbon background. Although the method described here for obtaining the few-layer graphene supports produces a mixture of graphite and graphene, the ease of fabrication and the opportunity to image on a near-backgroundless substrate outweigh the inconvenience of searching for few-layer graphene. Until large-area graphene is mass-produced cheaply, this method provides an economical and quick solution for those who are trying to image very small or amorphous species. As demonstrated by Meyer et al. (16), and in the results presented here, graphene has the potential to revitalize aging TEM systems, giving access to imaging capabilities unattainable using traditional support films.

Acknowledgment. Funding for this research was provided by Vanderbilt University, by The Vanderbilt Institute of Nanoscience and Engineering, and by the Division of Materials Science and Engineering of the U.S. Department of Energy. Some of the instrumentation used in this research was provided as part of the TEAM project, funded by the Department of Energy, Office of Science.

Supporting Information Available: Figures giving an RBS spectrum of $CuInSe_2$ nanocrystals and additional electron microscopy images. This material is available free of charge via the Internet at http://pubs.acs.org.

REFERENCES AND NOTES

(1) Murray, C. B.; Norris, D. J.; Bawendi, M. G. *J. Am. Chem. Soc.* **1993**, *115*, 8706–8715.
(2) Kadavanich, A. V. The Structure and Morphology of Semiconductor Nanocrystals; Ph.D. Thesis, University of California Berkeley, Berkeley, CA, 1997.
(3) Kadavanich, A. V.; Kippeny, T. C.; Erwin, M. M.; Pennycook, S. J.; Rosenthal, S. J. *J. Phys. Chem. B* **2001**, *105* (2), 361–369.
(4) McBride, J. R.; Kippeny, T. C.; Pennycook, S. J.; Rosenthal, S. J. *Nano Lett.* **2004**, *4* (7), 1279–1283.
(5) McBride, J.; Treadway, J.; Feldman, L. C.; Pennycook, S. J.; Rosenthal, S. J. *Nano Lett.* **2006**, *6* (7), 1496–1501.
(6) Peng, Z. A.; Peng, X. *J. Am. Chem. Soc.* **2001**, *123*, 1389–1395.
(7) Rosenthal, S. J.; McBride, J.; Pennycook, S. J.; Feldman, L. C. *Surf. Sci. Rep.* **2007**, *62*, 111–157.
(8) Ouyang, J.; Zaman, M. B.; Yan, F. J.; Johnston, D.; Li, G.; Wu, X.; Leek, D.; Ratcliffe, C. I.; Ripmeester, J. A.; Yu, K. *J. Phys. Chem. C* **2008**, *112* (36), 13805–13811.
(9) Peng, Z. A.; Peng, X. G. *J. Am. Chem. Soc.* **2002**, *124* (13), 3343–3353.
(10) Kudera, S.; Zanella, M.; Giannini, C.; Rizzo, A.; Li, Y. Q.; Gigli, G.; Cingolani, R.; Ciccarella, G.; Spahl, W.; Parak, W. J.; Manna, L. *Adv. Mater.* **2007**, *19* (4), 548–552.
(11) Micic, O. I.; Ahrenkiel, S. P.; Nozik, A. J. *Appl. Phys. Lett.* **2001**, *78* (25), 4022–4024.
(12) Riehle, F. S.; Bienert, R.; Thomann, R.; Urban, G. A.; Kruger, M. *Nano Lett.* **2009**, *9* (2), 514–518.
(13) Bowers, M. J., II; McBride, J. R.; Garrett, M. D.; Sammons, J. A.; Dukes, A. D., III; Schreuder, M. A.; Watt, T. L.; Lupini, A. R.; Pennycook, S. J.; Rosenthal, S. J. *J. Am. Chem. Soc.* **2009**, *131* (16), 5730–5731.
(14) Chen, X.; Samia, A. C. S.; Lou, Y.; Burda, C. *J. Am. Chem. Soc.* **2005**, *127*, 4372–4375.
(15) Novoselov, K. S.; Geim, A. K.; Morozov, S. V.; Jiang, D.; Zhang, Y.; Dubonos, S. V.; Grigorieva, I. V.; Firsov, A. A. *Science* **2004**, *306* (5296), 666–669.
(16) Meyer, J. C.; Girit, C. O.; Crommie, M. F.; Zettl, A. *Nature* **2008**, *454* (7202), 319–322.
(17) Silcox, J. *Nature* **2008**, *454* (7202), 283–284.
(18) Lee, Z.; Jeon, K.-J.; Dato, A.; Erni, R.; Richardson, T. J.; Frenklach, M.; Radmilovic, V. *Nano Lett.* **2009**, *9* (9), 3365–3369.
(19) Booth, T. J.; Blake, P.; Nair, R. R.; Jiang, D.; Hill, E. W.; Bangert, U.; Bleloch, A.; Gass, M.; Novoselov, K. S.; Katsnelson, M. I.; Geim, A. K. *Nano Lett.* **2008**, *8* (8), 2442–2446.
(20) Mkhoyan, K. A.; Contryman, A. W.; Silcox, J.; Stewart, D. A.; Eda, G.; Mattevi, C.; Miller, S.; Chhowalla, M. *Nano Lett.* **2009**, *9* (3), 1058–1063.
(21) Meyer, J. C.; Geim, A. K.; Katsnelson, M. I.; Novoselov, K. S.; Booth, T. J.; Roth, S. *Nature* **2007**, *446* (7131), 60–63.
(22) Gass, M. H.; Bangert, U.; Bleloch, A. L.; Wang, P.; Nair, R. R.; Geim, A. K. *Nature Nanotechnol.* **2008**, *3* (11), 676–681.
(23) Girit, C. O.; Meyer, J. C.; Erni, R.; Rossell, M. D.; Kisielowski, C.; Yang, L.; Park, C. H.; Crommie, M. F.; Cohen, M. L.; Louie, S. G.; Zettl, A. *Science* **2009**, *323* (5922), 1705–1708.
(24) Ferrari, A. C.; Meyer, J. C.; Scardaci, V.; Casiraghi, C.; Lazzeri, M.; Mauri, F.; Piscanec, S.; Jiang, D.; Novoselov, K. S.; Roth, S.; Geim, A. K. *Phys. Rev. Lett.* **2006**, *97* (18), 187401–187404.
(25) Novoselov, K. S.; Jiang, D.; Schedin, F.; Booth, T. J.; Khotkevich, V. V.; Morozov, S. V.; Geim, A. K. *Proc. Natl. Acad. Sci. USA* **2005**, *102* (30), 10451–10453.
(26) Blake, P.; Hill, E. W.; Neto, A. H. C.; Novoselov, K. S.; Jiang, D.; Yang, R.; Booth, T. J.; Geim, A. K. *Appl. Phys. Lett.* **2007**, *91* (6), 063124.
(27) Wang, J. J.; Zhu, M. Y.; Outlaw, R. A.; Zhao, X.; Manos, D. M.; Holloway, B. C.; Mammana, V. P. *Appl. Phys. Lett.* **2004**, *85* (7), 1265–1267.
(28) Chuang, A. T. H.; Boskovic, B. O.; Robertson, J. *Diamond Relat. Mater.* **2006**, *15* (4–8), 1103–1106.
(29) Antisari, M. V.; Montone, A.; Jovic, N.; Piscopiello, E.; Alvani, C.; Pilloni, L. *Scr. Mater.* **2006**, *55* (11), 1047–1050.
(30) Choucair, M.; Thordarson, P.; Stride, J. A. *Nature Nanotechnol.* **2009**, *4* (1), 30–33.
(31) Dato, A.; Radmilovic, V.; Lee, Z. H.; Phillips, J.; Frenklach, M. *Nano Lett.* **2008**, *8* (7), 2012–2016.
(32) Li, X. L.; Zhang, G. Y.; Bai, X. D.; Sun, X. M.; Wang, X. R.; Wang, E.; Dai, H. J. *Nature Nanotechnol.* **2008**, *3* (9), 538–542.
(33) Reina, A.; Jia, X. T.; Ho, J.; Nezich, D.; Son, H. B.; Bulovic, V.; Dresselhaus, M. S.; Kong, J. *Nano Lett.* **2009**, *9* (1), 30–35.
(34) Tung, V. C.; Allen, M. J.; Yang, Y.; Kaner, R. B. *Nature Nanotechnol.* **2009**, *4* (1), 25–29.
(35) Hernandez, Y.; Nicolosi, V.; Lotya, M.; Blighe, F. M.; Sun, Z. Y.; De, S.; McGovern, I. T.; Holland, B.; Byrne, M.; Gun'ko, Y. K.; Boland, J. J.; Niraj, P.; Duesberg, G.; Krishnamurthy, S.; Goodhue, R.; Hutchison, J.; Scardaci, V.; Ferrari, A. C.; Coleman, J. N. *Nature Nanotechnol.* **2008**, *3* (9), 563–568.
(36) Blake, P.; Brimicombe, P. D.; Nair, R. R.; Booth, T. J.; Jiang, D.; Schedin, F.; Ponomarenko, L. A.; Morozov, S. V.; Gleeson, H. F.; Hill, E. W.; Geim, A. K.; Novoselov, K. S. *Nano Lett.* **2008**, *8* (6), 1704–1708.

(37) Bowers, M. J., II; McBride, J. R.; Rosenthal, S. J. *J. Am. Chem. Soc.* **2005**, *127* (44), 15378–15379.
(38) Panthani, M. G.; Akhavan, V.; Goodfellow, B.; Schmidtke, J. P.; Dunn, L.; Dodabalapur, A.; Barbara, P. F.; Korgel, B. A. *J. Am. Chem. Soc.* **2008**, *130* (49), 16770–16777.
(39) Allen, P. M.; Bawendi, M. G. *J. Am. Chem. Soc.* **2008**, *130* (29), 9240–9241.
(40) Warner, J. H.; Schäffel, F.; Rümmeli, M. H.; Büchner, B. *Chem. Mater.* **2009**, *21* (12), 2418–2421.
(41) Swafford, L. Homogeneously Alloyed Cadmium Sulfoselenide Nanocrystals; Thesis; Vanderbilt University, Nashville, TN, 2006.
(42) Zimmer, J. P.; Kim, S.; Ohnishi, S.; Tanaka, E.; Frangioni, J. V.; Bawendi, M. G. *J. Am. Chem. Soc.* **2006**, *128*, 2526–2527.
(43) Dagtepe, P.; Chikan, V.; Jasinksi, J.; Leppert, V. J. *J. Phys. Chem. C* **2007**, *111* (41), 14977–14983.
(44) Kasuya, A.; Sivamohan, R.; Barnakov, Y. A.; Dmitruk, I. M.; Nirasawa, T.; Romanyuk, V. R.; Kumar, V.; Mamykin, S. V.; Tohji, K.; Jeyadevan, B.; Shinoda, K.; Kudo, T.; Terasaki, O.; Liu, Z.; Belosludov, R. V.; Sundararajan, V.; Kawazoe, Y. *Nat. Mater.* **2004**, *3* (2), 99–102.
(45) Jose, R.; Zhanpeisov, N. U.; Fukumura, H.; Baba, Y.; Ishikawa, M. *J. Am. Chem. Soc.* **2006**, *128* (2), 629–636.
(46) Deglmann, P.; Ahlrichs, R.; Tsereteli, K. *J. Chem. Phys.* **2002**, *116* (4), 1585–1597.
(47) Eichkorn, K.; Ahlrichs, R. *Chem. Phys. Lett.* **1998**, *288* (2−4), 235–242.
(48) Troparevsky, M. C.; Chelikowsky, J. R. *J. Chem. Phys.* **2001**, *114* (2), 943–949.
(49) Yu, Z. H.; Guo, L.; Du, H.; Krauss, T.; Silcox, J. *Nano Lett.* **2005**, *5* (4), 565–570.
(50) Carlson, L. J.; Maccagnano, S. E.; Zheng, M.; Silcox, J.; Krauss, T. D. *Nano Lett.* **2007**, *7* (12), 3698–3703.
(51) Tang, J.; Hinds, S.; Kelley, S. O.; Sargent, E. H. *Chem. Mater.* **2008**, *20* (22), 6906–6910.
(52) Xie, R. G.; Rutherford, M.; Peng, X. G. *J. Am. Chem. Soc.* **2009**, *131* (15), 5691–5697.
(53) Garrett, M. D.; Dukes, A. D.; McBride, J. R.; Smith, N. J.; Pennycook, S. J.; Rosenthal, S. J. *J. Phys. Chem. C* **2008**, *112* (33), 12736–12746.

AM900608J